Direct Simulation Monte-Carlo prediction of coarse elastic particle statistics in fully developed turbulent channel flows: comparison with deterministic discrete particle simulation results and moment closure assumptions

Pascal Fede, Olivier Simonin

Direct Simulation Monte-Carlo predictions of coarse elastic particle statistics in fully developed turbulent channel flows: Comparison with deterministic discrete particle simulation results and moment closure assumptions

Pascal Fede*, Olivier Simonin

Institut de Mécanique des Fluides de Toulouse (IMFT), Université de Toulouse, CNRS, Toulouse, France

Keywords:
DSMC
Gas-particle vertical flow
Second-order moment method

A B S T R A C T

The paper presents numerical simulations of particle-laden fully developed turbulent channel flows performed in a stochastic Lagrangian framework. The particle inertia is large in order to neglect the effect of the turbulent gas motion on the particle dispersion. In contrast the inter-particle collisions are important and accounted for by using Direct Simulation Monte-Carlo (DSMC) method. The comparison of the Monte-Carlo results with those obtained by Discrete Particle Simulation (DPS) shows that the stochastic collisions algorithm is able to predict accurately the particle statistics (number density, mean velocity, second- and third-order velocity moments) in the core flow. More, the paper analyses the number sections needed for accurate predictions. In the very near-wall region, the Monte-Carlo simulation fails to account for the wall shelter effect due to the wall-normal unbalanced inter-particle collisions influence induced by the presence of the wall. Then, the paper shows that DSMC permits to assess the closure approximations required in moment approach. In particular, the DSMC results are compared with the corresponding moment closure assumptions for the third-order correlations of particle velocity, the correlations between the drag force and the velocity and the inter-particle collision terms. It is shown that at the opposite of the standard DSMC, the moment approach can predict the wall shelter effect. Finally, a model for the mean transverse force is proposed for taking into account wall shelter effect in DSMC.

1. Introduction

Particle-laden flows are found in a large spectrum of practical applications ranging from geophysical flows (sediment transport, pyroclastic flow, volcano ashes dispersion...) to industrial applications (solid or liquid fuel combustor, catalytic reactor, spray tower, solid handling,...) and passing through medical applications (room disinfection, medicament aerosol inhalation,...). In isothermal particle-laden flows, many complex phenomena take place, such as turbulent dispersion, inter-particle collisions, particle bouncing with smooth or rough walls, or turbulence modulation by the particles who need to be accurately modelled.

Because of the discrete nature of the particles, the numerical simulation of the particle motion is widely performed in a Lagrangian framework by Discrete Particle Simulation (DPS). That approach can be either coupled with Direct Numerical Simulation (DPS/DNS), Large Eddy Simulation (DPS/LES) or Reynolds Averaged Navier–Stokes approach (DPS/RANS) (Sommerfeld, 2001; Riber et al., 2009; Balachandar and Eaton, 2010; Fox, 2012; Capecelatro and Desjardins, 2013). When the collisions are treated in a deterministic manner, DPS/DNS can be considered as full deterministic numerical simulation approach because no stochastic model for both particle turbulent dispersion and inter-particle collisions are needed. In contrast, for DPS/LES and DPS/RANS, a stochastic dispersion model is needed to account for the subgrid (LES), or the fluctuating (RANS), fluid velocity along the particle trajectories. In practical applications, due to the huge number of real particles, the computation of all individual particle trajectories is not possible but this difficulty can be overtaken in the frame of Lagrangian statistical approaches leading to replace the real particles by a reduced number of parcels representing several real particles.

Stochastic Lagrangian algorithms were first derived for the collisions of molecules in rarefied gases (Bird, 1969; Babovsky, 1986). In the framework of DPS/RANS approach these algorithms were used for taking into account the inter-particle collisions in gas-particle turbulent flows (O'Rourke, 1981; Tanaka and Tsuji, 1991).

* Corresponding author.
E-mail address: pascal.fede@imft.fr (P. Fede).

https://doi.org/10.1016/j.ijmultiphaseflow.2018.06.005

However, several studies have shown some problems related to the effect of the turbulence on the colliding particles (Berlemont et al., 1995; Sommerfeld, 2001; Berlemont et al., 2001; Wang et al., 2009; Pawar et al., 2014; Fede et al., 2015; He et al., 2015; Tsirkunov and Romanyuk, 2016).

In the present paper, Monte-Carlo algorithm is used to account for the inter-particle collisions in a vertical turbulent channel flows. Then the DSMC method is assessed by comparison with statistics from DPS where the fluid flow is steady and imposed (Sakiz and Simonin, 1998; 1999b; 1999a). In such a case, the particle inertia is sufficiently large so that the effect of the turbulence on the particle motion can be neglected. More, the solid mass loading is small in order to neglect the turbulence modulation by the presence of the particles. Hence, the proposed simulation method is developed in the frame of DPS/RANS approach where the fluid velocity is known and predicted by the standard $k-\varepsilon$ model. The particles dynamic is controlled by the competition between the entrainment by the mean fluid flow and the inter-particle collisions. In Section 4, the results given by the stochastic algorithm are assessed by comparison with the deterministic DPS predictions. A very good agreement is found between both simulation methods, except in the very near-wall region where the deterministic simulations exhibit a "wall shelter effect" that cannot be accounted for by using the standard DSMC method.

Following Fede et al. (2015), DSMC methods are Lagrangian stochastic methods developed for the numerical solution of the Eulerian kinetic equation governing the particle velocity Probability Density Function (Reeks, 1991) or the particle-fluid joint PDF (Simonin, 1996). An other method to compute the particle statistics consists in the numerical solution of governing equations derived from the PDF kinetic equation for several low-order particle velocity moments (number density, mean velocity, fluctuant kinetic energy, ...) Such an approach, commonly called Eulerian approach or moment method, leads to solve a set of Eulerian transport equations and needs to develop additional closure modelling assumptions for the gas-particle and particle-particle interaction terms and for the high-order velocity moment representing the kinetic dispersion (transport by the particle velocity fluctuations). In the present study, DSMC results are used to analyse the closure models for the drag, the turbulent dispersion and the collisions derived in the frame of second order moment methods.

After the introduction, the paper gives the configuration and details the investigated cases. The third section is dedicated to the statistical approaches for turbulent gas–solid flows. The focus is made on the DSMC algorithm for taking into account the inter-particle collisions. The DSMC results are analysed in the fourth section by comparison with deterministic simulations. The analysis of second order moment closures from DSMC results is given in the fifth section. A model for taking into account the "wall shelter effect" in DSMC is proposed. The paper ends by concluding remarks.

2. Configuration overview

2.1. Fluid flow

The flow configuration is a fully developed vertical gas–solid turbulent channel flow (Sakiz and Simonin, 1998; 1999a; 1999b). As shown by Fig. 1, the computational domain is a rectangular box with periodic boundary conditions in the streamwise and spanwise directions.

According to the large particle inertia and to the low solid mass loading, the particle interaction with the fluid turbulence and the modification of the mean fluid flow by the particles (two-way coupling) were neglected. Therefore, in this work, the fluid velocity is a given mean field taken from $k-\epsilon$ model predictions of fully developed turbulent channel single-phase flow. The material properties of the fluid are $\rho_f = 1.205\,\mathrm{kg/m^3}$ an $\nu_f = 1.515\times10^{-5}\,\mathrm{m^2/s}$.

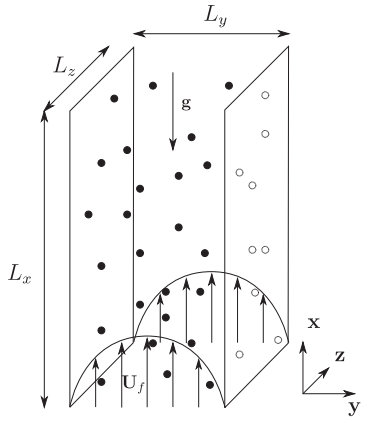

Fig. 1. Flow configuration with $L_x = 240$ mm, $L_y = 40$ mm, and $L_z = 32$ mm.

Table 1
Particle material properties. The mean solid volume volume fraction is computed as $\overline{\alpha_p} = N_p\pi d_p^3/6/V$ with N_p the total number of tracked particles in DPS and V the volume of the computational domain.

d_p µm	ρ_p [kg/m^3]	$\overline{\alpha_p}$	N_p
200	1038	5×10^{-4}	31,000
406	1038	1.2×10^{-3}	9000
406	1038	4×10^{-3}	29,600
406	1038	10^{-2}	73,800
1500	1032	4.1×10^{-3}	600
1500	1032	1.4×10^{-2}	2000
1500	1032	4.1×10^{-2}	6000

2.2. Particle motion

The particles are assumed spherical with a diameter d_p and with a large particle-to-fluid density ratio (see Table 1). In such a framework, only the drag force and the gravity are acting on the particles motion. Introducing $\mathbf{u}_p$, the particle translation velocity and $\mathbf{u}_{f@p}$, the fluid velocity seen by the particle, the particle velocity momentum equation reads

$$\frac{d\mathbf{u}_p}{dt} = \frac{\mathbf{F}_d}{m_p} = -\frac{\mathbf{u}_p - \mathbf{u}_{f@p}}{\tau_p} + \mathbf{g} \tag{1}$$

where $\mathbf{F}_d$ is the instantaneous drag force acting on a single particle, $\mathbf{g}$ the gravity acceleration, and τ_p the instantaneous particle response time given by

$$\tau_p = \frac{4}{3}\frac{\rho_p}{\rho_g}\frac{d_p}{C_D}\frac{1}{|\mathbf{v}_r|}\ . \tag{2}$$

In Eq. (2), $\mathbf{v}_r = \mathbf{u}_p - \mathbf{u}_{f@p}$ is the instantaneous gas-particle relative velocity, ρ_p the particle density. The drag coefficient, C_D, is given in terms of particle Reynolds number (Schiller and Naumann, 1935),

$$C_D = \frac{24}{Re_p}\left[1 + 0.15Re_p^{0.687}\right] \tag{3}$$

with $Re_p = d_p|\mathbf{v}_r|/\nu_g$. As the gas turbulence and the two-way coupling are both neglected, the instantaneous fluid velocity seen by the particle is obtained by an interpolation of the given mean fluid velocity field at the particle centre position: $\mathbf{u}_{f@p} = \mathbf{U}_f(\mathbf{x}_p)$.

2.3. Inter-particle and particle-wall collision

In the present study the particle volume fractions are sufficiently low in order that only binary collisions are taken into ac-

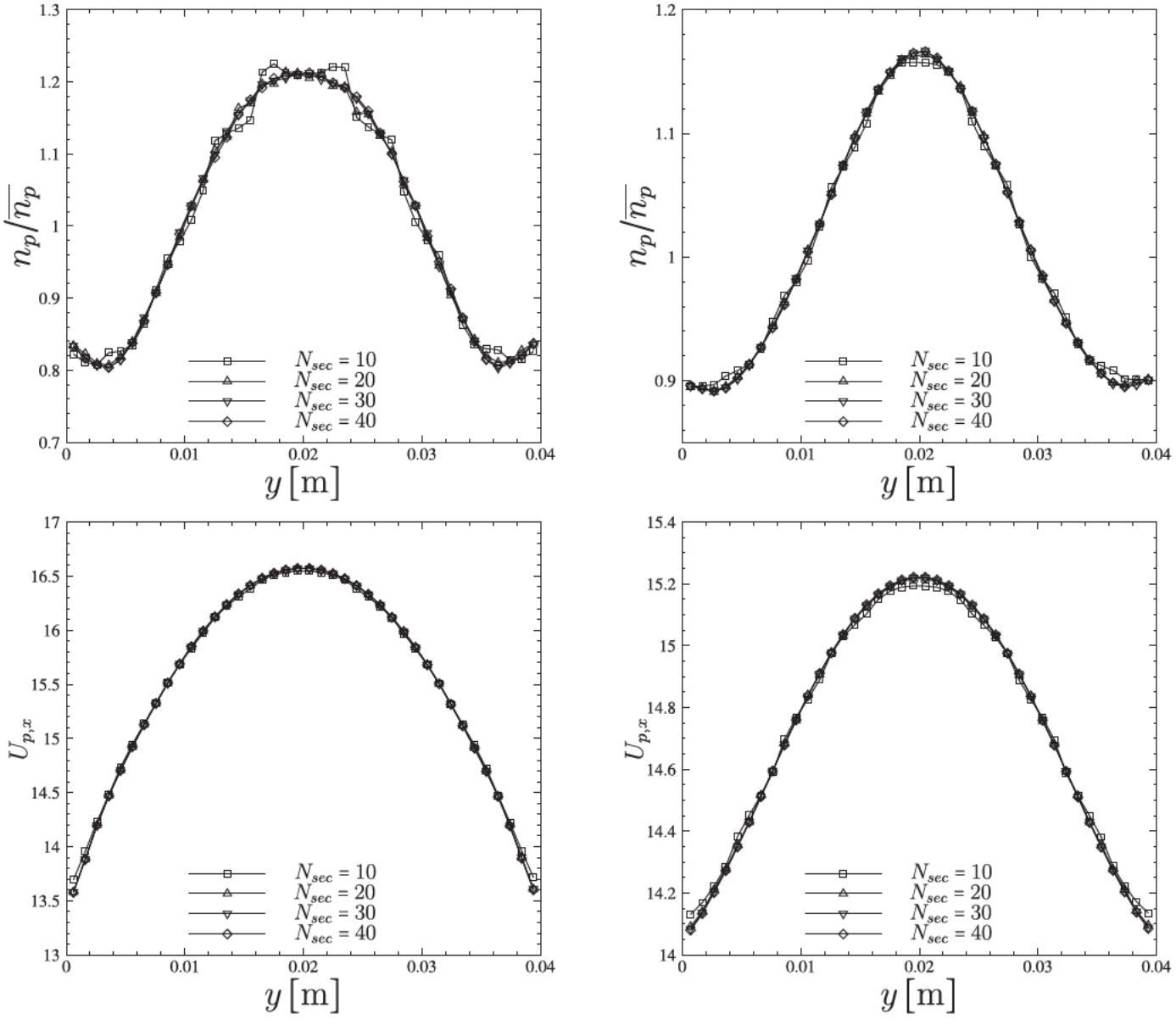

Fig. 2. Effect of the number of sections used for the DSMC for a fixed number of parcels ($N_{par} = 10,000$). The left column corresponds to the case where $d_p = 200$ µm & $\overline{\alpha_p} = 5.0 \times 10^{-4}$ and the right column to the case where $d_p = 406$ µm & $\overline{\alpha_p} = 10^{-2}$. Top: Mean particle density number an bottom: mean vertical particle velocity.

count. Considering a collision between a particle p and a particle q, the unit vector linking the centre of the p-particle to the one of the q-particle is $\mathbf{k}$ and the inter-particle relative velocity is $\mathbf{w} = \mathbf{u}_q - \mathbf{u}_p$. Neglecting the inter-particle friction, the velocities after a collision are given by

$$\mathbf{u}_p^* = \mathbf{u}_p + \frac{1+e_c}{2}(\mathbf{w}.\mathbf{k})\mathbf{k} \tag{4}$$

$$\mathbf{u}_q^* = \mathbf{u}_q - \frac{1+e_c}{2}(\mathbf{w}.\mathbf{k})\mathbf{k}. \tag{5}$$

where e_c is the inter-particle restitution coefficient. The particle-wall interactions are considered fully elastic without friction. Then the particle velocity after wall bouncing reads $\mathbf{u}_p^* = \mathbf{u}_p - 2(\mathbf{u}_p.\mathbf{n}_w)\mathbf{n}_w$ where $\mathbf{n}_w$ is the unit vector normal to the wall.

3. Statistical modelling approaches

3.1. Statistical description

The statistical description of the dispersed phase, composed of solid particles transported by a turbulent fluid flow, relies on the analogy with the thermal motion of molecules as described by the kinetic theory of rarefied gases (Chapman and Cowling, 1970; Jenkins and Richman, 1985) and later extended for turbulent gas-particle flows (Reeks, 1991; Simonin, 2000; Zaichik et al., 2004; Reeks et al., 2016). In the statistical approach, the dispersed phase is described by the particle Probability Density Function $f_p(\mathbf{c}_p, \mathbf{x}; t)$ defined such that $f_p(\mathbf{c}_p, \mathbf{x}; t)d\mathbf{c}_p d\mathbf{x}$ is the mean probable number of particles at time t with the centre of mass, $\mathbf{x}_p$, located in the volume $[\mathbf{x}, \mathbf{x} + d\mathbf{x}]$, and the translation velocity, $\mathbf{u}_p$, within $[\mathbf{c}_p, \mathbf{c}_p + d\mathbf{c}_p]$. From the PDF definition the number density of particles writes

$$n_p(\mathbf{x}, t) = \int f_p(\mathbf{c}_p, \mathbf{x}; t)\, \mathbf{c}_p, \tag{6}$$

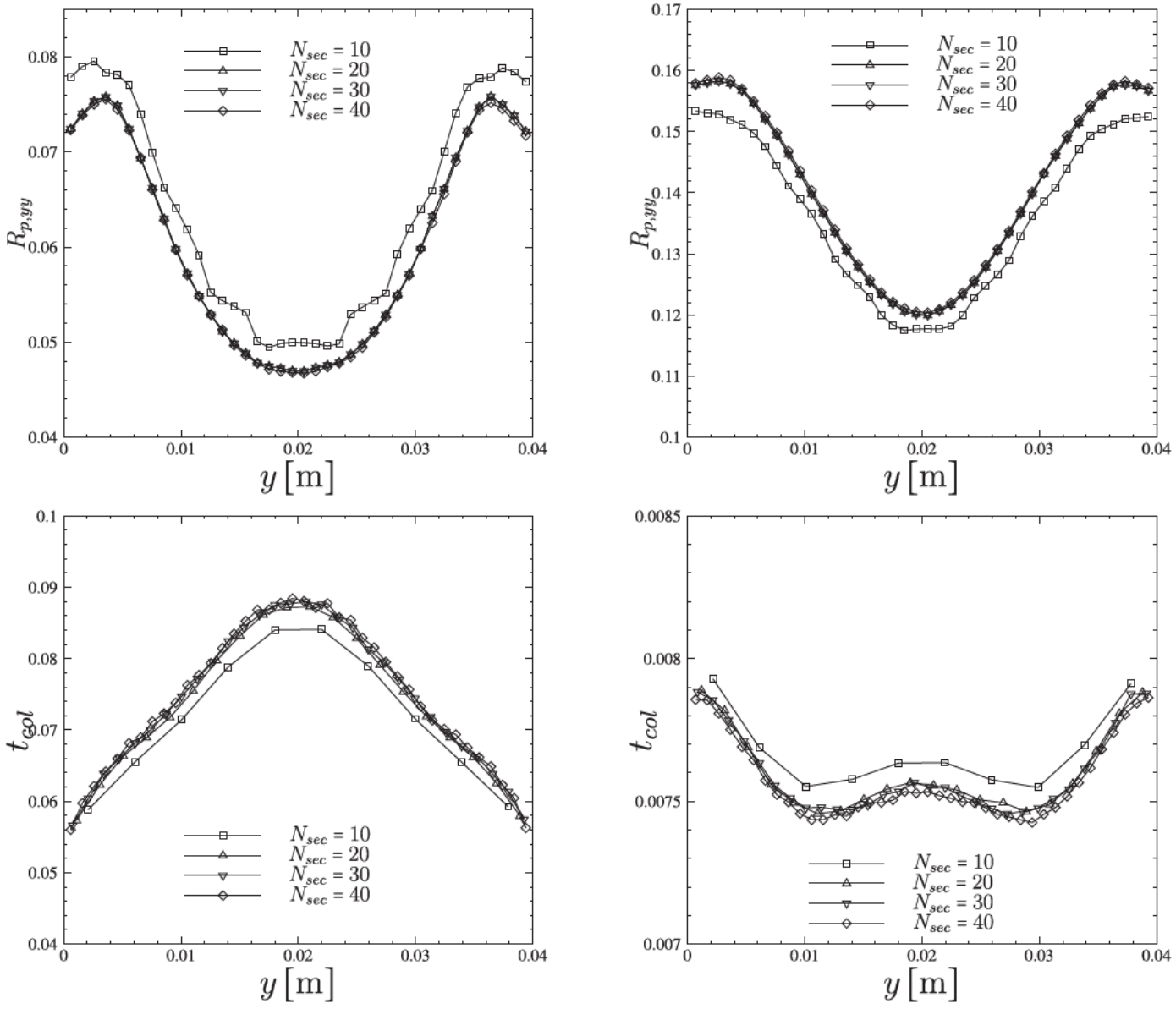

Fig. 3. Effect of the number of sections used for the DSMC for a fixed number of parcels ($N_{par} = 10,000$). The left column corresponds to the case where $d_p = 200$ μm & $\overline{\alpha_p} = 5.0 \times 10^{-4}$ and the right panel to the case where $d_p = 406$ μm & $\overline{\alpha_p} = 10^{-2}$. Top: wall-normal component of the particle kinetic stress and bottom: inter-particle collision timescale.

the mean particle velocity,

$$U_{p,i}(\mathbf{x},t) = \frac{1}{n_p}\int c_{p,i} f_p(\mathbf{c}_p,\mathbf{x};t)\, d\mathbf{c}_p \ , \tag{7}$$

the particle kinetic stress tensor $R_{p,ij} = \langle u'_{p,i} u'_{p,j} \rangle$,

$$R_{p,ij} = \frac{1}{n_p}\int [c_{p,i} - U_{p,i}] \times [c_{p,j} - U_{p,j}] f_p(\mathbf{c}_p,\mathbf{x};t)\, d\mathbf{c}_p \ , \tag{8}$$

and the third-order particle velocity correlation $S_{p,ijk} = \langle u'_{p,i} u'_{p,j} u'_{p,k} \rangle$,

$$S_{p,ijk} = \frac{1}{n_p}\int [c_{p,i} - U_{p,i}] \times [c_{p,j} - U_{p,j}] \times [c_{p,k} - U_{p,k}] f_p(\mathbf{c}_p,\mathbf{x};t)\, d\mathbf{c}_p. \tag{9}$$

The PDF of single particle velocity obeys the following Boltzmann-like kinetic equation:

$$\frac{\partial f_p}{\partial t} + \frac{\partial}{\partial x_i}\left[c_{p,i} f_p\right] + \frac{\partial}{\partial c_{p,i}}\left[\left\langle \frac{du_{p,i}}{dt} | \mathbf{c}_p \right\rangle f_p\right] = \left.\frac{\partial f_p}{\partial t}\right|_{col} \tag{10}$$

where $\langle . | \mathbf{c}_p \rangle$ is the ensemble average conditioned by the particle velocity, $\mathbf{u}_p = \mathbf{c}_p$. The third term on the left-hand side of Eq. (10) represents the forces acting on the particles, enclosing the turbulent particle-fluid coupling. As the effect of the turbulence on the particle motion is neglected, this term is directly written as

$$\frac{\partial}{\partial c_{p,i}}\left[\left\langle \frac{du_{p,i}}{dt} | \mathbf{c}_p \right\rangle f_p\right] = \frac{\partial}{\partial c_{p,i}}\left[\left(-\frac{c_{p,i} - U_{f,i}}{\tau_p} + g_i\right) f_p\right] \tag{11}$$

where $U_{f,i}(\mathbf{x},t)$ is the mean fluid velocity. In Eq. (10) the term on the right-hand side represents the modification of the PDF by the inter-particle collisions.

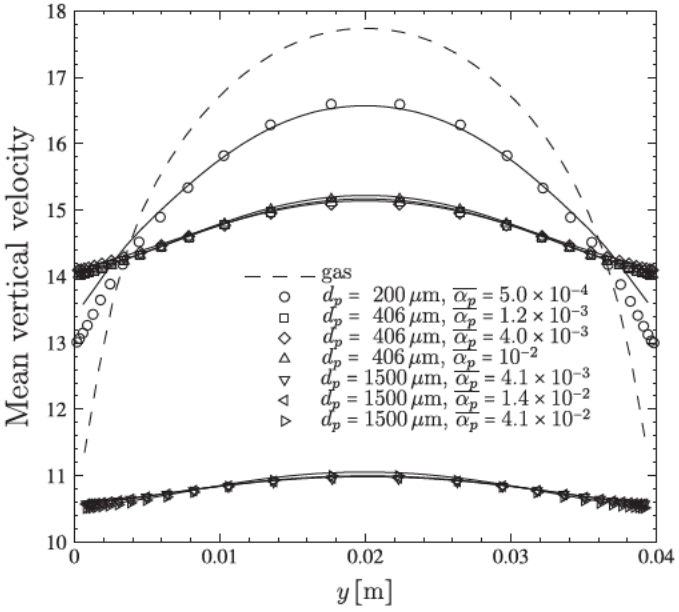

Fig. 4. Gas and particle mean vertical velocities for several particle diameters and mean solid volume fractions. The symbols are the DPS results from Sakiz and Simonin (1998) and the solid lines (——) are the DSMC results.

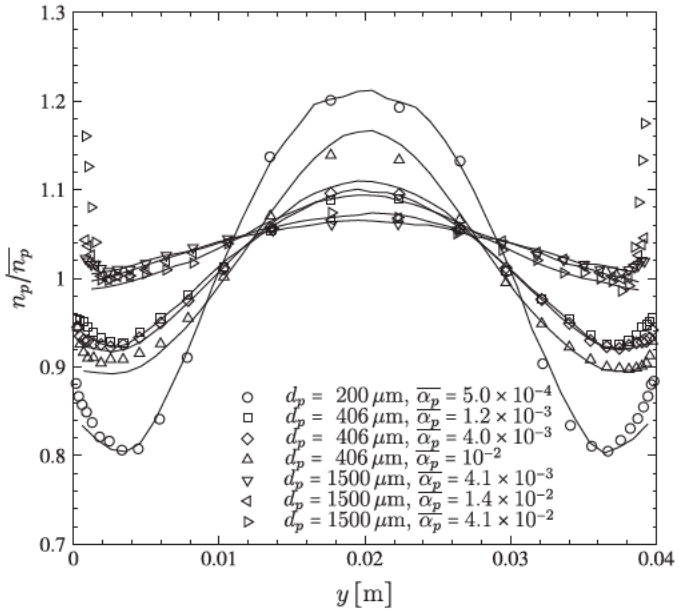

Fig. 5. Particle number density normalized by the average value over the whole domain for several particle diameters and volume fractions. The symbols are the DPS results from Sakiz and Simonin (1998) and the solid lines (——) are the DSMC results.

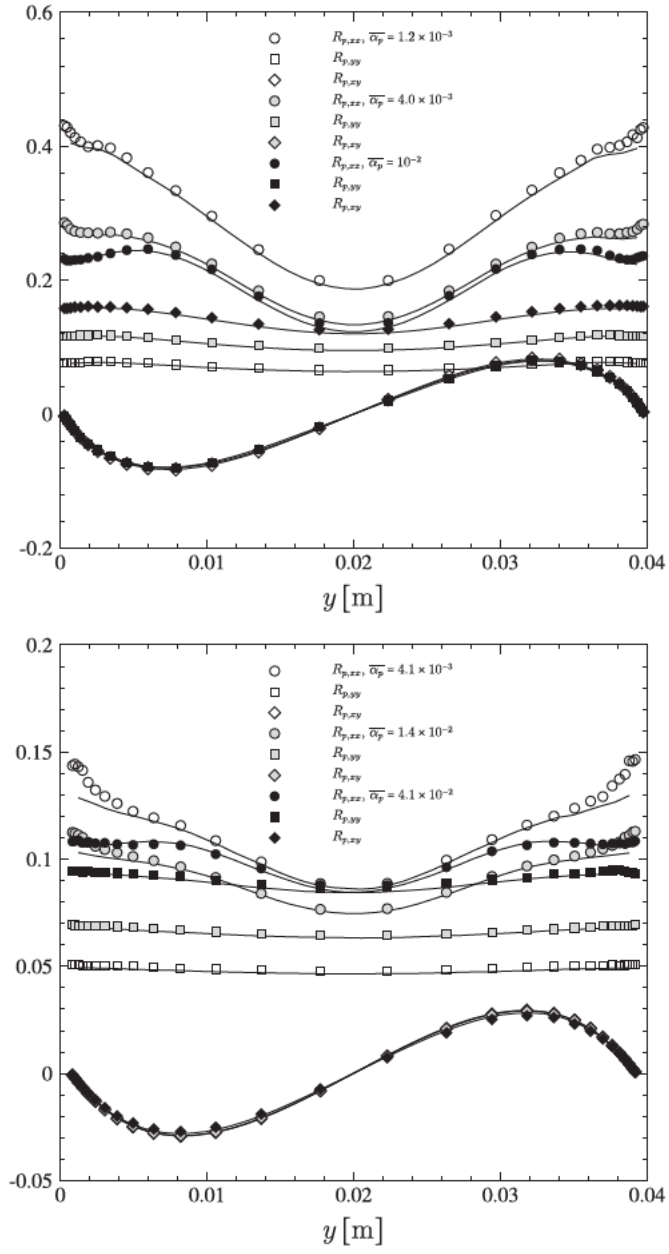

Fig. 6. Mean particle kinetic stress components for $d_p = 406$ μm (top) and $d_p = 1500$ μm (bottom). The symbols are the DPS results from Sakiz and Simonin (1998) and the solid lines (——) are the DSMC results.

3.2. Monte-Carlo algorithm

Stochastic particle methods, also called Monte-Carlo methods or Direct Simulation Monte-Carlo (DSMC), were initially developed for solving the Boltzmann equation for rarefied gas dynamics (Bird, 1969; Nanbu, 1983; Babovsky, 1986; Ivanov and Rogasinsky, 1988; Sommerfeld, 2001; Arcen et al., 2006; Fede et al., 2015). Basically, these methods approximate the PDF as:

$$f_p(\mathbf{c}_p, \mathbf{x}; t) = \sum_{i=1}^{N_{par}(t)} w_p^i \delta\left[\mathbf{x} - \mathbf{x}_p^i\right] \times \delta\left[\mathbf{c}_p - \mathbf{u}_p^i\right] . \quad (12)$$

Such an approximation commonly introduces the idea that the particles are represented by "numerical particles" or "parcels" that are a group of w_p^i of real particles located around the same space position, and having the same velocity. An important feature of stochastic particle methods is the use of a fractional time step algorithm, which consists in splitting each time step in the two following substeps:

- a transport substep corresponding to the discretization of the free flight of parcels, i.e. the non-collisional kinetic equation. During this substep the position, velocity of each numerical particle are updated by solving the particle motion equations.
- a collision substep which corresponds to the discretization of the collision term. The mesh cells have to be small enough for the exact PDF to be almost uniform over them so that

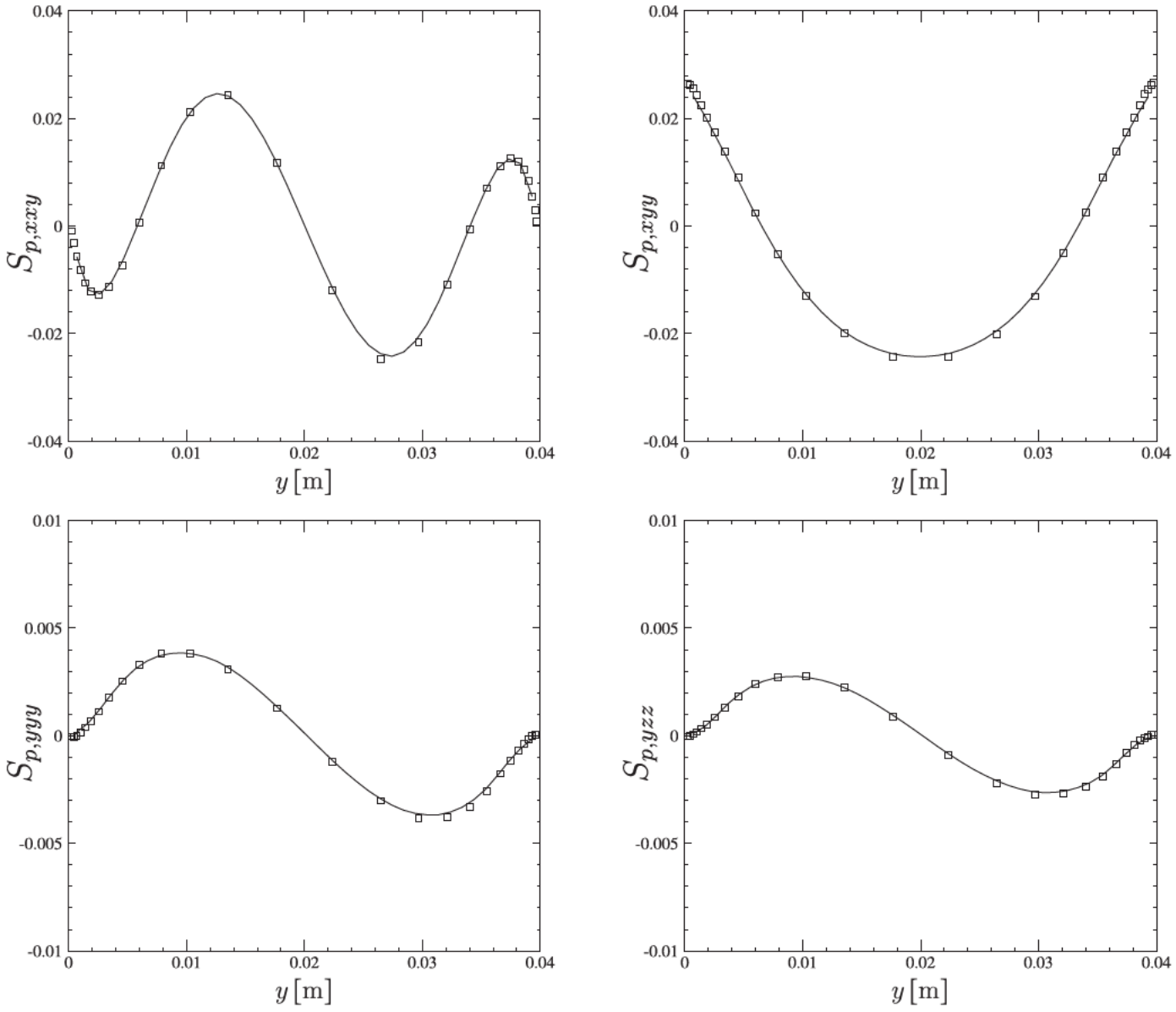

Fig. 7. Third order correlations for $d_p = 406$ µm and $\overline{\alpha_p} = 1.2 \times 10^{-3}$. The symbols are the DPS results from Sakiz and Simonin (1998) and the solid lines (——) are the DSMC results.

Eq. (12) could be replaced by:

$$f_p(\mathbf{c}_p, \mathbf{x}; t) = \sum_{C_i} \sum_{k \in Ind(C_i)} w_p^k \frac{\mathbf{1}_{C_i}(\mathbf{x})}{vol(C_i)} \delta\left[\mathbf{c}_p - \mathbf{u}_p^k\right] \tag{13}$$

where C_i denotes a given cell of the mesh $\mathcal{M}_x$, $\mathbf{1}_{C_i}$ is the indicator function of C_i (top-hat distribution function), $Ind(C_i)$ is the list of parcels located in cell C_i at the end of the transport step and $vol(C_i)$ is the volume of C_i. From a physical point of view, this new approximation of the PDF means that, during the collision substep, all real particles represented by a given parcel are supposed to be randomly distributed in the cell containing the parcel instead of being all located at the same point as during the transport step. The collision substep then consists in applying a Monte-Carlo algorithm for computing in each cell an approximate solution of the spatially homogeneous Boltzmann equation:

$$\frac{\partial f_p}{\partial t}(\mathbf{c}_p, \mathbf{x}; t) = Q_{coll}\{f_p\}(\mathbf{c}_p, \mathbf{x}; t), \tag{14}$$

assuming that the initial PDF can be approximated by (13). It is worth noticing that the expression of Q_{coll} in Eq. (14) relies on a closure assumption for the pair PDF which may be based on the molecular chaos assumption for very inertial particles with respect to the turbulent time macroscale (Simonin et al., 2002; Fede et al., 2015).

In DSMC method the wall boundary conditions for the particles are the same than those used in DPS.

The domain is uniformly discretized in 10 to 40 N_{sec} vertical sections for the collision substep where local homogeneous random particle distribution is assumed. While computation of the particle statistics is carried out by averaging Lagrangian predictions on a given number of sections ($N_y = 40$). The total number of parcels is the same for all cases and set to $N_{par} = 10{,}000$. Figs. 2 and 3 show the effect of the section number N_{sec} on the predictions of the particle number density and of the first and second-order velocity moments. Fig. 2 shows that particle number density and mean vertical velocity predictions are mesh independent from a relatively low number of sections: $N_{sec} = 10$. In

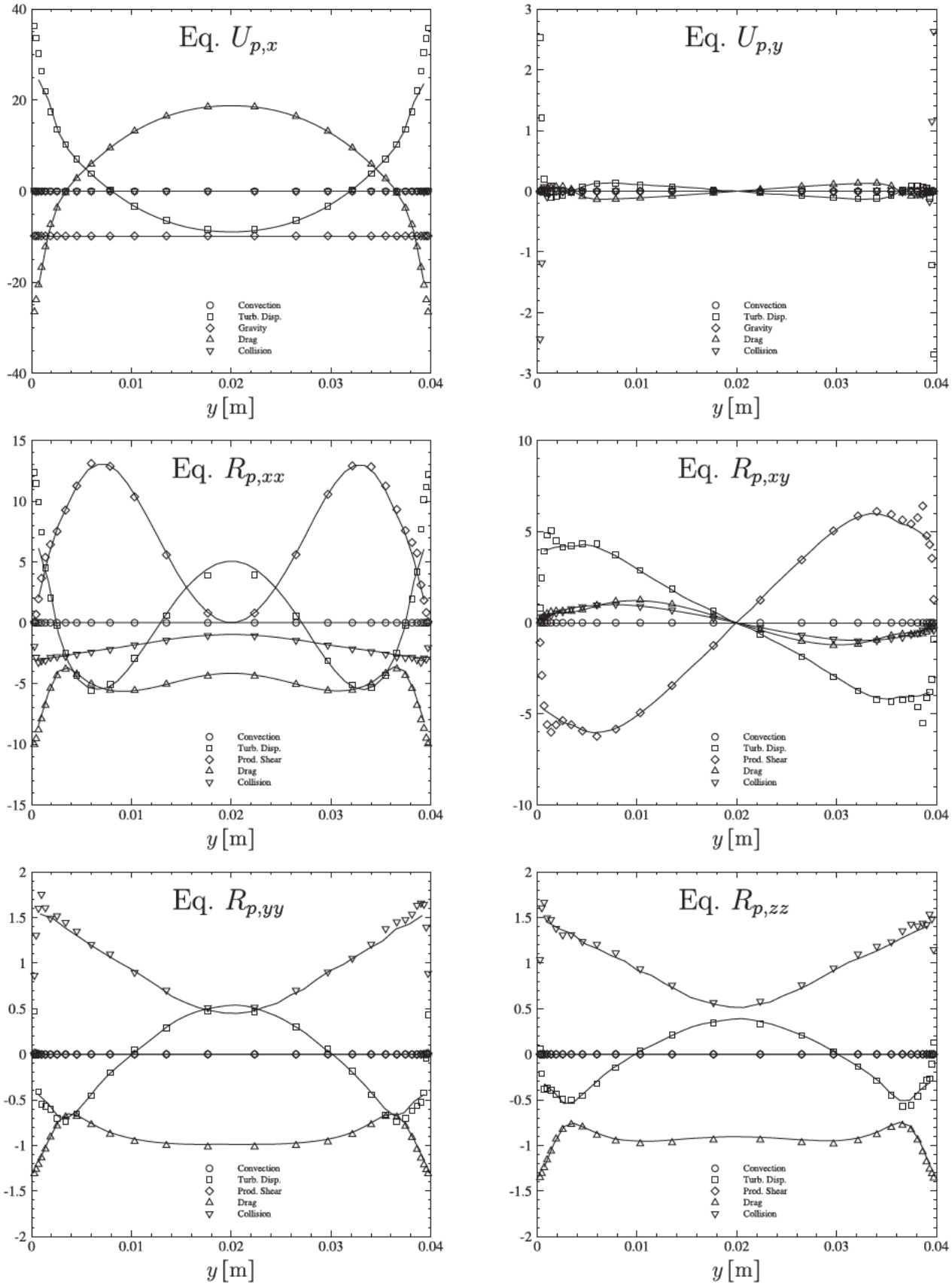

Fig. 8. Budget of moment equations for the case $d_p =$ 406 μm and $\overline{\alpha_p} = 1.2 \times 10^{-3}$. The symbols are the DPS results from Sakiz and Simonin (1998) and the solid lines (_____) are the DSMC results.

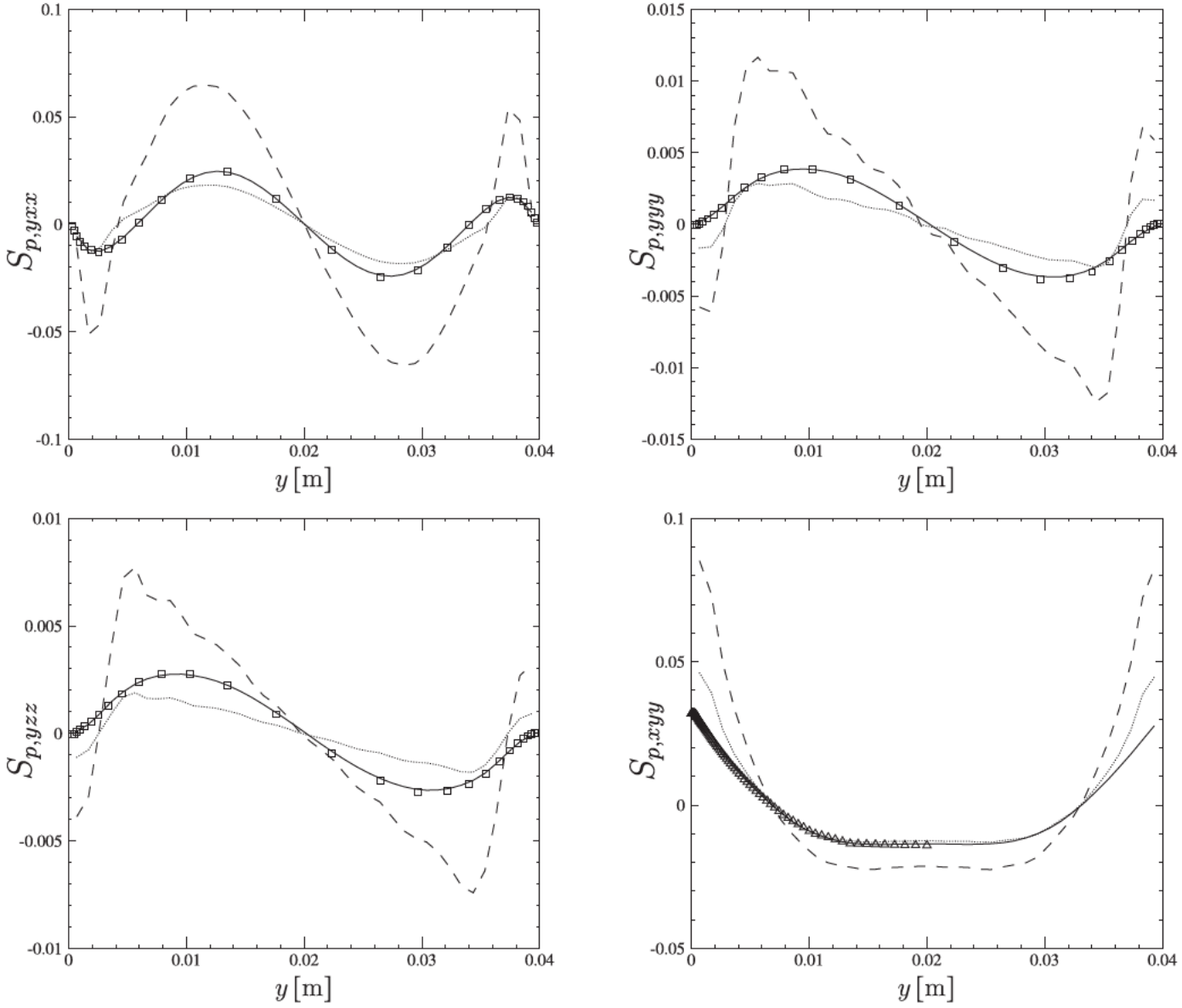

Fig. 9. Third order correlation $S_{p,\,ijk}$ for the case $d_p = 406$ µm and $\overline{\alpha_p} = 1.2\ 10^{-3}$. The symbols are the DPS results from Sakiz and Simonin (1998) (if available), the solid lines (_____) are the DSMC results, the dashed lines (_ _ _) the moment method modelling using Eqs. (22) and (23) and the dotted lines (.....) the moment method modelling using Eqs. (22) and (24).

contrast, Fig. 3 shows that the wall normal particle kinetic stress, $R_{p,\,yy}$, and the collision timescale predictions are more dependent on the number of sections. We can notice that for the smallest number of sections, $N_{sec} = 10$, the wall normal kinetic stress is slightly over-predicted for the small particles, $d_p = 200$ µm, and under-predicted for the large ones, $d_p = 406$µm. Finally, the predictions are nearly independent of the mesh for $N_{sec} \geq 20$, therefore the specific value $N_{sec} = 30$ is used for the predictions presented in the paper.

3.3. Moment approach

From the PDF kinetic equation (Eq. (10)), it is possible to derive the transport equation of each moment of the PDF (Simonin, 1996) by multiplying Eq. (10) by a polynomial function of the velocity components and integrating over all particle velocity expectations. According to Sakiz and Simonin (1998), without particle deposition or resuspension, for sufficient long time, the periodic discrete particle simulation in the vertical channel leads to a fully developed particle flow with velocity moments verifying: $U_{p,y} = 0$ and $\partial/\partial t \equiv \partial/\partial x \equiv \partial/\partial z \equiv 0$. The number density balance equation writes

$$\frac{\partial}{\partial y}(n_p U_{p,y}) = 0\ . \tag{15}$$

The mean particle velocity equations read

$$\frac{\partial U_{p,x}}{\partial t} = -\frac{1}{n_p}\frac{\partial}{\partial y}(n_p R_{p,xy}) - g + \left\langle \frac{F_{d,x}}{m_p} \right\rangle + \frac{1}{n_p} C(u_{p,x}), \tag{16}$$

$$\frac{\partial U_{p,y}}{\partial t} = -\frac{1}{n_p}\frac{\partial}{\partial y}(n_p R_{p,yy}) + \left\langle \frac{F_{d,y}}{m_p} \right\rangle + \frac{1}{n_p} C(u_{p,y})\ . \tag{17}$$

As the flow is fully developed, the time derivative in Eqs. (16) and (17) is zero but it has been kept in order to clearly identify the mean velocity component which obeys to the corresponding equation. The first term on the right-hand side is the kinetic dispersion, the two following terms are the gravity and the drag force terms.

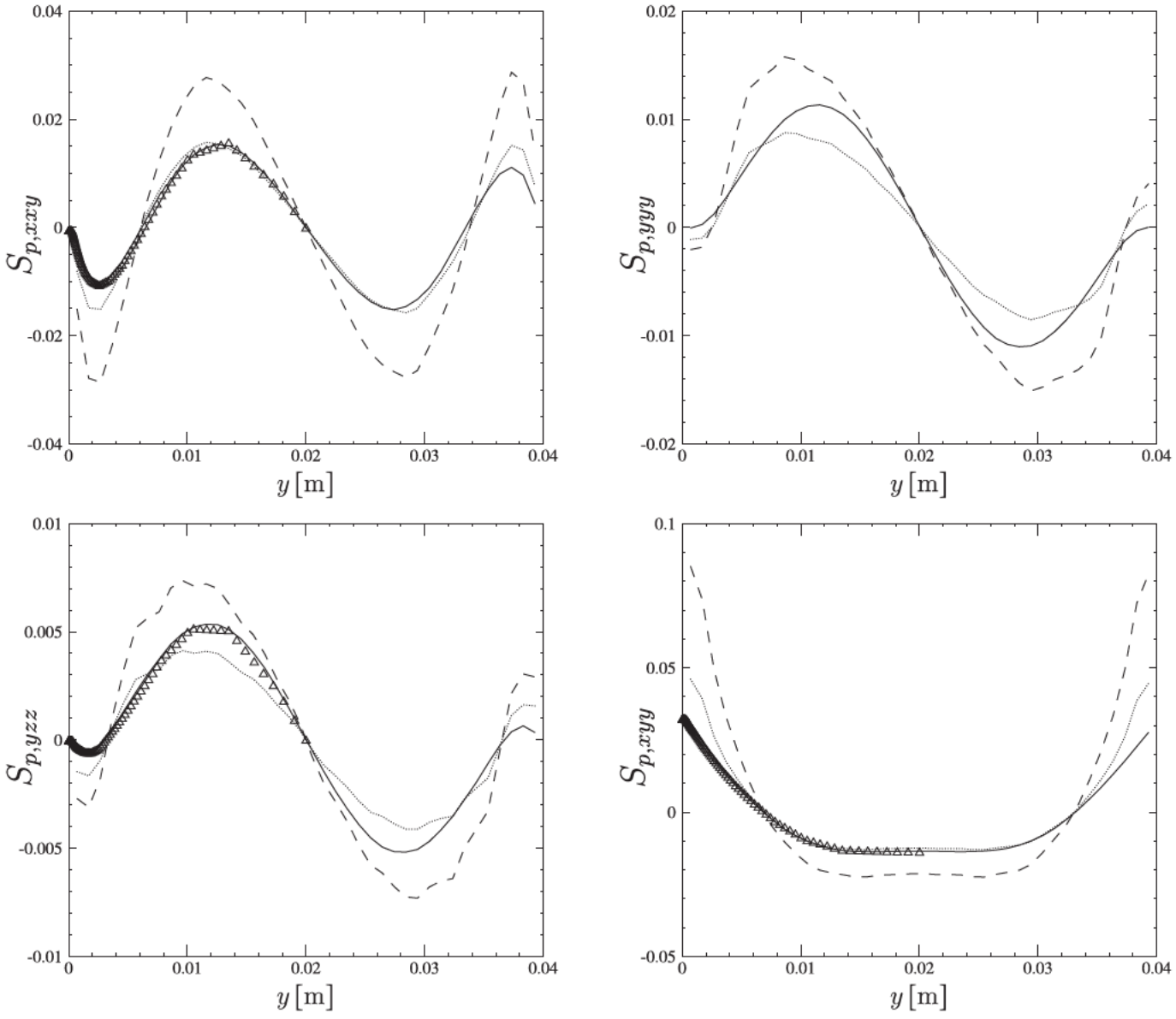

Fig. 10. Third order correlation $S_{p,\,ijk}$ for the case $d_p = 406$ μm and $\overline{\alpha_p} = 10^{-2}$. The symbols are the DPS results from Sakiz and Simonin (1998) (if available), the solid lines (_____) are the DSMC results, the dashed lines (_ _ _) the moment method modelling using Eqs. (22) and (23) and the dotted lines (.....) the moment method modelling using Eqs. (22) and (24).

Finally, the last term represents the effect of the inter-particle collisions.

The particle kinetic stress tensor component (or centered second-order velocity moment) transport equations are written

$$\frac{\partial R_{p,xx}}{\partial t} = -\frac{1}{n_p}\frac{\partial}{\partial y}(n_p S_{p,xxy}) - 2R_{p,xy}\frac{\partial U_{p,x}}{\partial y} + 2\left\langle \frac{F_{d,x}}{m_p}u'_{p,x}\right\rangle + \frac{1}{n_p}\mathcal{C}(u'_{p,x}u'_{p,x}), \tag{18}$$

$$\frac{\partial R_{p,yy}}{\partial t} = -\frac{1}{n_p}\frac{\partial}{\partial y}(n_p S_{p,yyy}) + 2\left\langle \frac{F_{d,y}}{m_p}u'_{p,y}\right\rangle + \frac{1}{n_p}\mathcal{C}(u'_{p,y}u'_{p,y}), \tag{19}$$

$$\frac{\partial R_{p,zz}}{\partial t} = -\frac{1}{n_p}\frac{\partial}{\partial y}(n_p S_{p,yzz}) + 2\left\langle \frac{F_{d,z}}{m_p}u'_{p,z}\right\rangle + \frac{1}{n_p}\mathcal{C}(u'_{p,z}u'_{p,z}), \tag{20}$$

$$\frac{\partial R_{p,xy}}{\partial t} = -\frac{1}{n_p}\frac{\partial}{\partial y}(n_p S_{p,xyy}) - R_{p,yy}\frac{\partial U_{p,x}}{\partial y} + \left[\left\langle \frac{F_{d,y}}{m_p}u'_{p,x}\right\rangle + \left\langle \frac{F_{d,x}}{m_p}u'_{p,y}\right\rangle\right] + \frac{1}{n_p}\mathcal{C}(u'_{p,x}u'_{p,y}). \tag{21}$$

As the flow is steady, the time derivative in Eqs. (18)–(21) is zero but it has been kept in order to clearly identify the kinetic stress tensor component which obeys the corresponding equation. The first term on the right-hand side of Eqs. (18)–(21) is the kinetic transport (see Section 5.1). The second term is the production by the shear of the mean particle velocity. The third term represents the effect of the drag force (see Section 5.2) and the last term represents the effect of the inter-particle collisions (see Section 5.3).

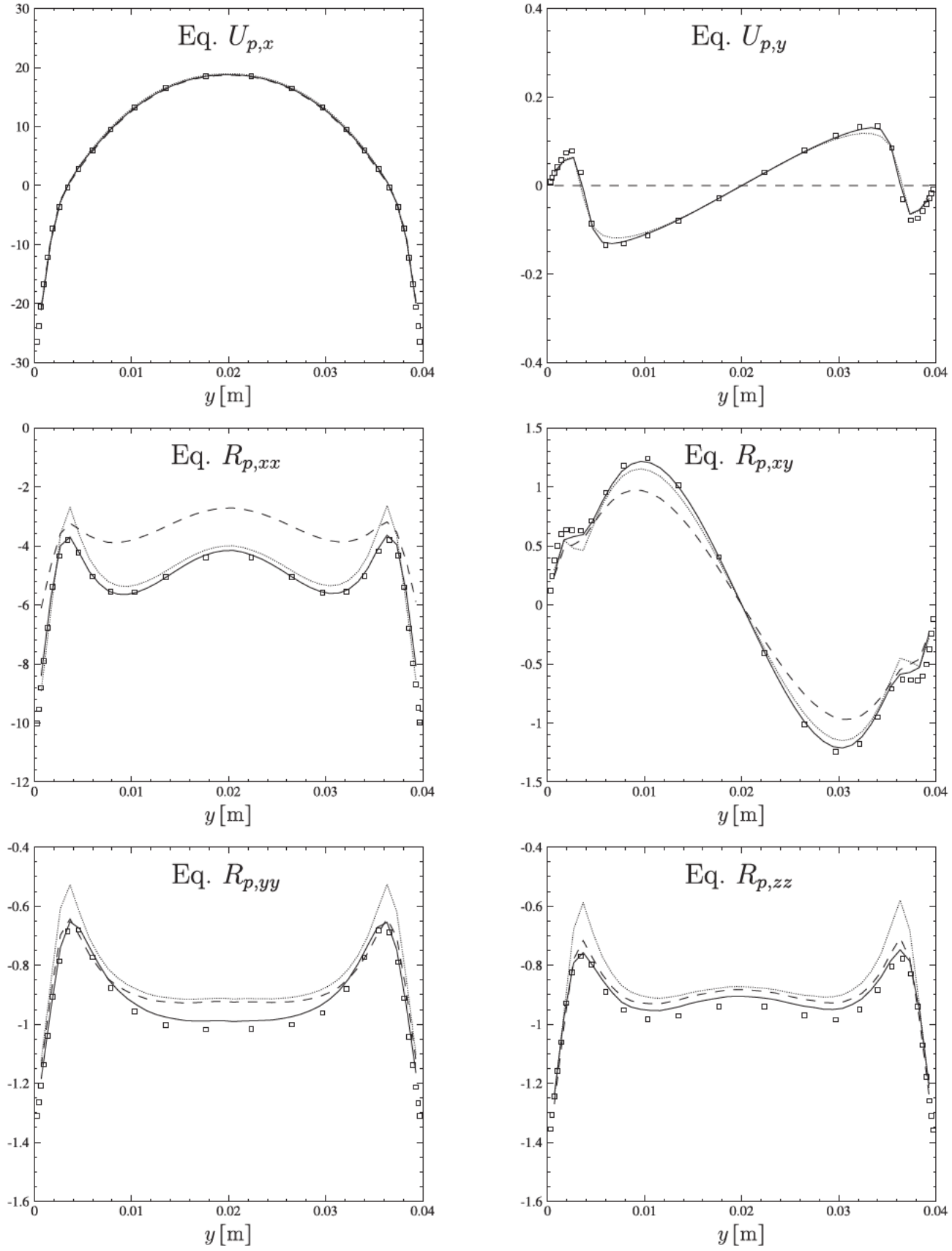

Fig. 11. A priori test of the drag term for the case $d_p =$ 406 µm and $\overline{\alpha_p} = 1.2 \times 10^{-3}$. The symbols are the DPS results from Sakiz and Simonin (1998), the solid lines (——) are the DSMC results, the dashed lines (– – –) the "standard" moment closure assumption of the drag (Eqs. (26) and (27)) and the dotted lines (.....) the extension proposed by Sakiz and Simonin (1998) including large drift effect (Eqs. (28) and (29)).

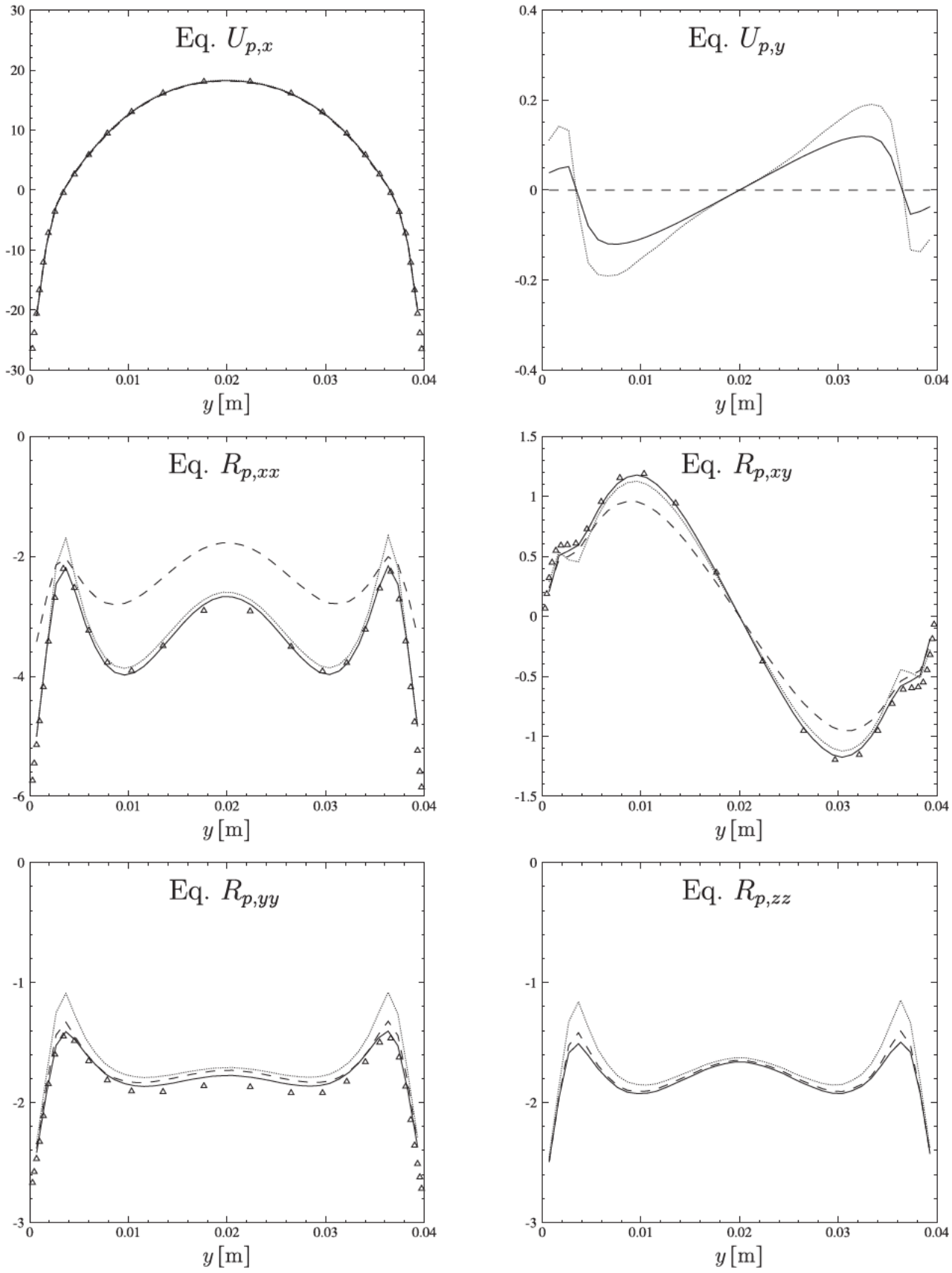

Fig. 12. A priori test of the drag term for the case $d_p =$ 406 μm and $\overline{\alpha_p} = 10^{-2}$. The symbols are the DPS results from Sakiz and Simonin (1998), the solid lines (_____) are the DSMC results, the dashed lines (_ _ _) the "standard" moment closure assumption of the drag (Eqs. (26) and (27)) and the dotted lines (.....) the extension proposed by Sakiz and Simonin (1998) including large drift effect (Eqs. (28) and (29)).

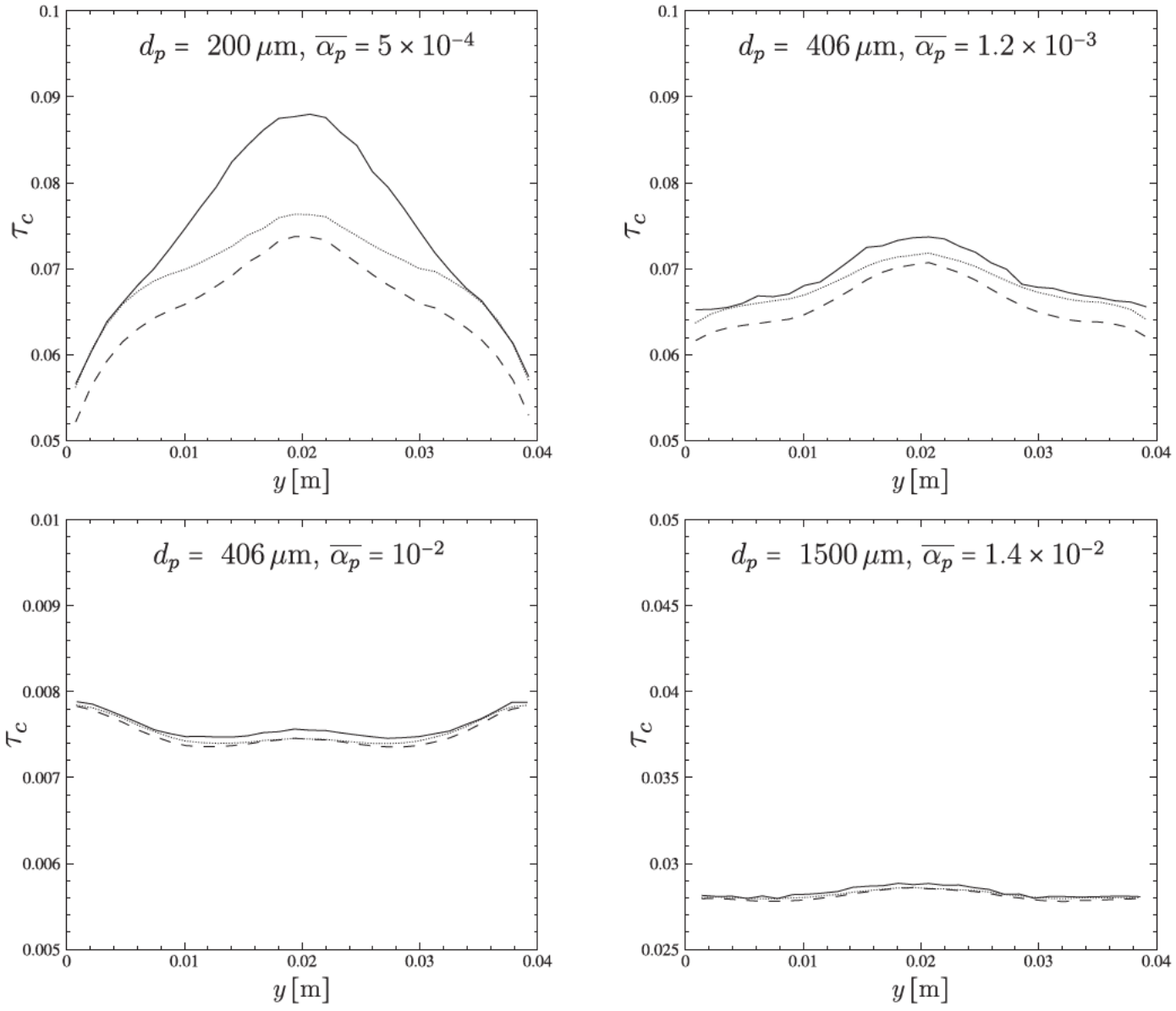

Fig. 13. Wall-normal distribution of collision time scale. The solid lines (_____) are the DSMC results, the dashed lines (_ _ _) the moment method modelling with Eq. (30) and the dotted line (.....) with Eq. (31).

4. DSMC results and discussion

All Monte-Carlo simulations have been made with the same number of sections $N_{sec} = 30$ of constant size. The mesh for computing the statistics is also uniform with $N_y = 40$ sections from $d_p/2$ to $L_y - d_p/2$. In all cases the number of parcel is the same $N_{par} = 10{,}000$. After a transient phase of 5 s the statistics are computed during 35 s.

Fig. 4 shows the mean gas and particle vertical velocities for several mean particle volume fractions and particle material properties. First of all, it can be observed that the mean particle volume fraction does not have a strong effect on the profiles of the mean particle velocity. At the channel centre, the mean vertical particle velocity is found always smaller than the fluid velocity and, as expected because of the gravity, the larger is the diameter the lower is the particle velocity. Close to the walls the vertical velocity of the particles with $d_p = 1500$ µm is always found smaller than the mean vertical gas velocity. In contrast, for $d_p = 200$ µm and $d_p = 406$ µm, Fig. 4 shows that the mean vertical particle velocity is larger than the fluid one. The equilibrium between these two regions is controlled by the wall-normal kinetic dispersion leading to a much flat profile for particle than for the gas.

As shown by Fig. 4, the DSMC predictions of the mean particle velocity are in very good agreement with the DPS results. Only slight differences can be observed in the near-wall regions.

The DSMC prediction of the particles number density across the channel is shown by Fig. 5. One can observed that the particle number density profiles exhibit a maximum at the channel centre. When approaching the wall, the particle number density decreases for reaching a minimum. Finally, for the smaller diameters ($d_p = 200$ µm and $d_p = 406$ µm), the particle number density computed from the DSMC results increases up to the wall. For $d_p = 1500$ µm the profiles of n_p are found slightly flatter indicating a larger efficiency of the dispersion in wall-normal direction as shown by the velocity profiles too. For the large particles with $d_p = 1500$ µm, Fig. 5 shows large discrepancies between the DSMC and DPS particle number density predictions in the near-wall region. As a matter of fact, the DPS results show a strong increase of

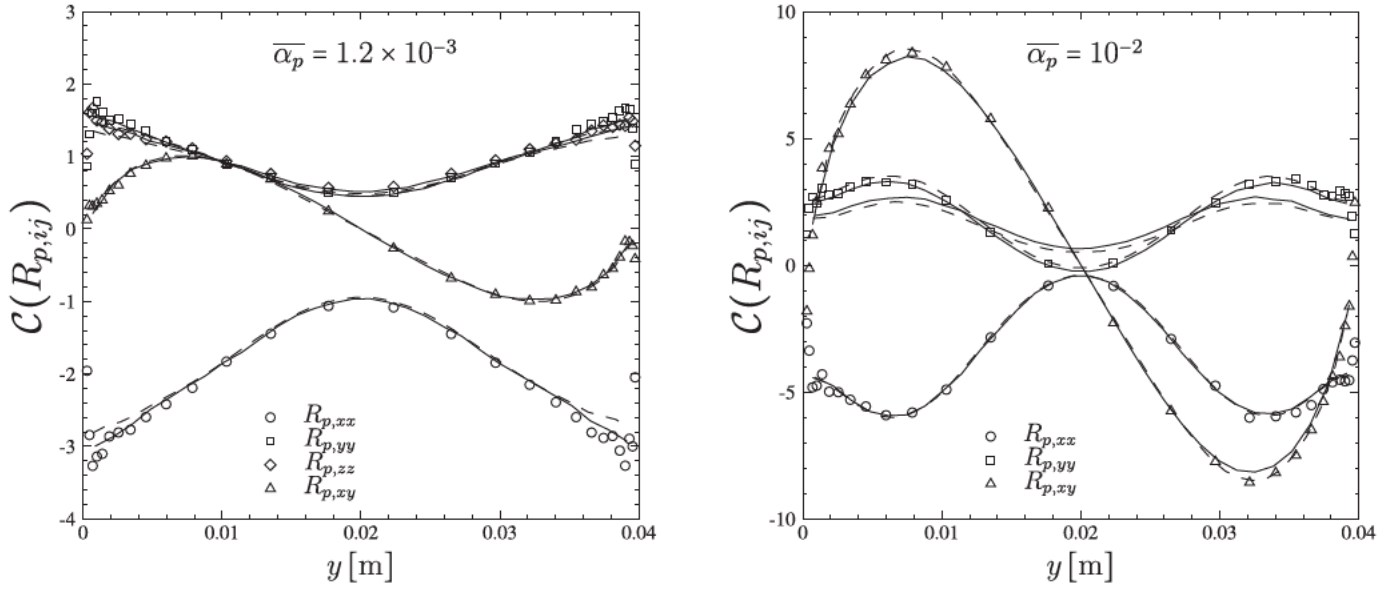

Fig. 14. A priori test of the collision term in transport equation of the second order particle velocity correlation for the case of $d_p = 406$ µm. The symbols are the DPS results from Sakiz and Simonin (1998), the solid lines (———) are the DSMC results, the dashed lines (– – –) the moment method predictions by Eq. (32) and (30).

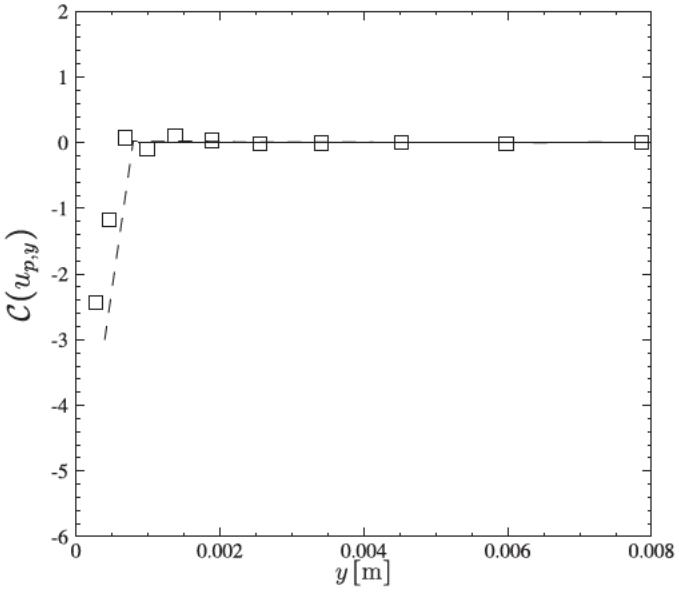

Fig. 15. A priori test of collision term in $U_{p,y}$ moment equation for the case $d_p = 406$ µm, $\overline{\alpha_p} = 1.2 \times 10^{-3}$. The symbols are the DPS results from Sakiz and Simonin (1998), the solid lines (———) the DSMC results and the dashed lines (– – –) the moment method modelling with Eq. (33). In such a case the number of sections for computing the statistics is $N_y = 100$.

the particle number density when approaching the wall and this peculiar behaviour is not captured by the DSMC method. Following Sakiz and Simonin (1998), this effect comes from the fact that the momentum transfer by inter-particle collision is unbalanced for particles sheltered by the wall closeness. It results a mean effective force towards the wall leading to an increase of the particle number density. This effect, called here "wall shelter effect", is found to be effective only when the particle centre to wall distance is smaller than $3/2d_p$.

The time-averaged components of the particle kinetic stress tensor components (or second order velocity correlations) measured in DPS and predicted by the stochastic Lagrangian simulations are shown by Fig. 6. It can be observed that the predictions of the DSMC method are in very good agreement with the DPS results. Fig. 6 shows that the fluctuating motion of the particles is anisotropic because of the production by the gradient of the mean particle velocity and a weak redistribution effect from the vertical velocity variance towards the horizontal ones. It can also be observed that when the solid volume fraction is increasing the anisotropy is decreasing (Fig. 7).

Fig. 8 shows a comparison between the DSMC and the DPS results of each term from the moment equations Eqs. (16)–(21).

5. Evaluation of closure assumptions for second-order moment transport equation

5.1. Triple velocity correlation closure moment

As shown by Eqs. (18)–(21), the second order moment approach requires closure assumptions for the third order particle fluctuating velocity correlations $S_{p,\,ijk}$. Following Simonin (1996) and Sakiz and Simonin (1999b), such a closure assumption can be obtained by writing the transport equation of the third order correlation $S_{p,\,ijk}$ for steady flow conditions. Several additional assumptions are necessary as the effect of the turbulence and the production by the gradients of the mean particle velocity are neglected. Then, the fourth-order correlation, $Q_{p,\,ijkl}$, is approximated assuming a Gaussian distribution leading to write the fourth-order correlation in terms of the second-order correlations. Finally a Grad's approximation (Grad, 1949) is used for writing the collision terms in the equation of $S_{p,\,ijk}$.

Hence, similarly to the model proposed (Hanjalic and Launder, 1972) for single-phase turbulent flows, the third order correlation can be written as:

$$S_{p,ijk} = -K_{p,in}\frac{\partial R_{p,jk}}{\partial x_n} - K_{p,jn}\frac{\partial R_{p,ik}}{\partial x_n} - K_{p,kn}\frac{\partial R_{p,ij}}{\partial x_n} \tag{22}$$

where the particle dispersion coefficient reads

$$K_{p,ij} = \left[\frac{3}{\tau_{fp}^F} + \frac{2}{3}\frac{\xi_c}{\tau_c}\right]^{-1} R_{p,ij} \tag{23}$$

and $\xi_c = (1+e_c)(49-33e_c)/60$ is a model constant depending on the inter-particle collision restitution coefficient e_c.

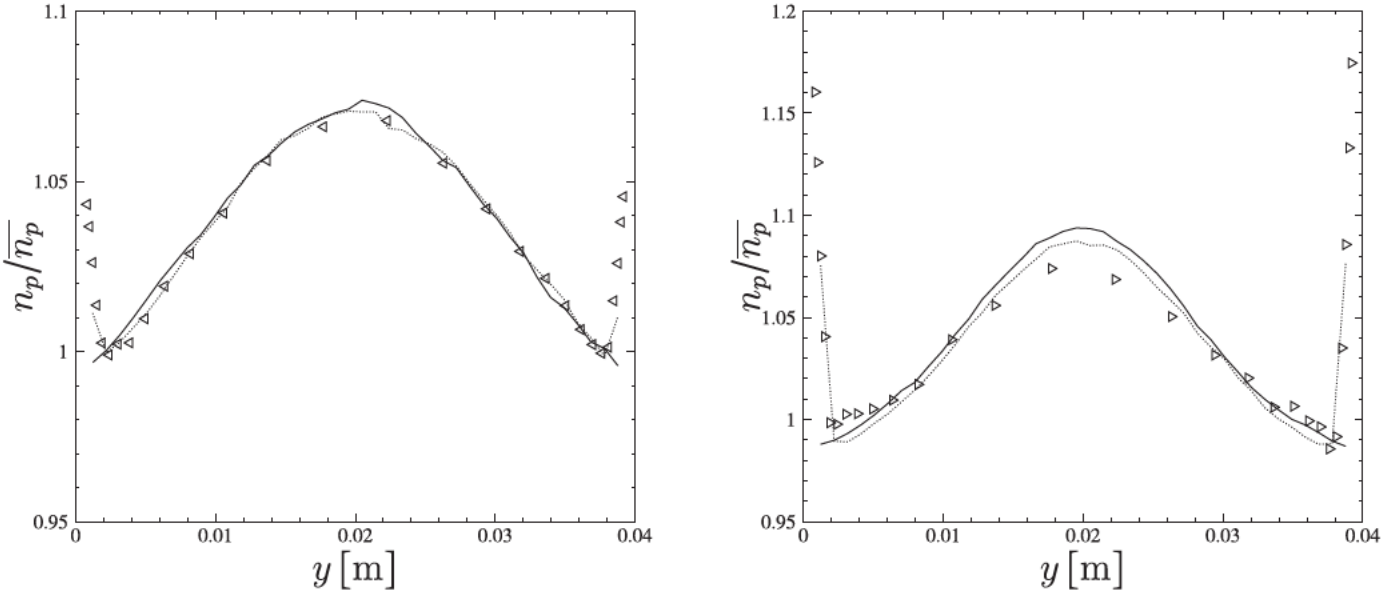

Fig. 16. Particle number density normalized by the average value over the whole domain for the case $d_p =$ 1500 μm (left: $\overline{\alpha_p} = 1.4 \times 10^{-2}$ and right: $\overline{\alpha_p} = 4.1 \times 10^{-2}$). The symbols are the DPS results from Sakiz and Simonin (1998), the solid lines (_____) the standard DSMC results and the dotted lines (.....) the DSMC results with the "wall force" given by Eq. (34).

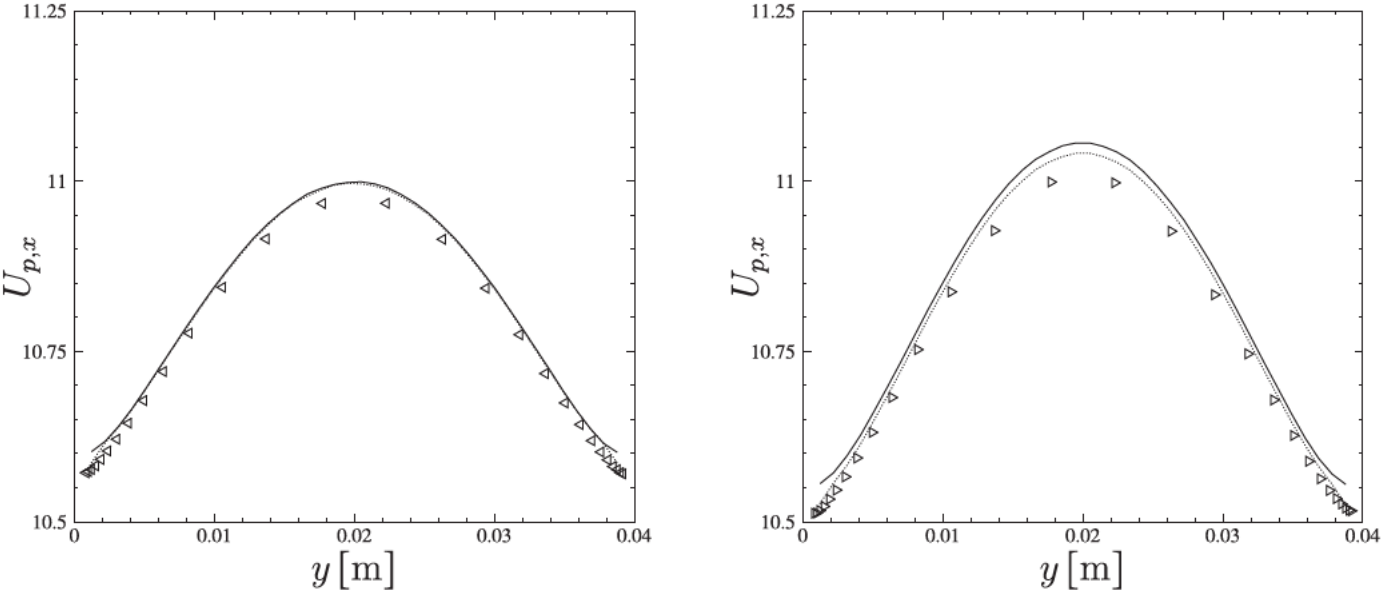

Fig. 17. Particle vertical velocity for the case $d_p =$ 1500 μm. Left: $\overline{\alpha_p} = 1.4 \times 10^{-2}$ and right: $\overline{\alpha_p} = 4.1 \times 10^{-2}$. The symbols are the DPS results from Sakiz and Simonin (1998), the solid lines (_____) the standard DSMC results and the dotted lines (.....) the DSMC results with the "wall force" given by Eq. (34).

Figs. 9 and 10 show the third-order correlations, appearing in the kinetic stress transport Eqs. (18)–(21), for the case with $d_p =$ 406 μm. As already shown, it can be denoted the remarkably accordance between the DPS and DSMC results. The moment closure assumptions of $S_{p,\,ijk}$ using Eqs. (22) and (23) are also shown by Figs. 9 and 10.

Figs. 9 and 10 show that the moment closure approach allows to reproduce roughly the shape of triple velocity correlation radial profiles given by DPS or DSMC and the agreement between moment closure approach and simulation results is increasing with respect to the volume fraction. Therefore, the measured discrepancies maybe interpreted as an overestimation of the dispersion coefficient given by Eq. (23). According to Sakiz and Simonin (1999a), this effect is due to the fact that inter-particle collision time τ_c is not sufficiently small, compared to the particle relaxation time, τ_{fp}^F, and to the mean particle transit time across the channel τ_p^K ($\tau_p^K = L_y / \overline{R_{p,yy}}$, where L_y is the width of the channel) to allow the collision process to counterbalance non-equilibrium effects induced by the interaction with the fluid and by the wall confinement. Following Sakiz and Simonin (2001), a semi-empirical correction of the dispersion coefficient is proposed to account for the non-equilibrium effect,

$$K_{p,ij} = \frac{1}{C}\left(\frac{3}{\tau_{fp}^F} + \frac{2}{3}\frac{\xi_c}{\tau_c}\right)^{-1} R_{p,ij} \tag{24}$$

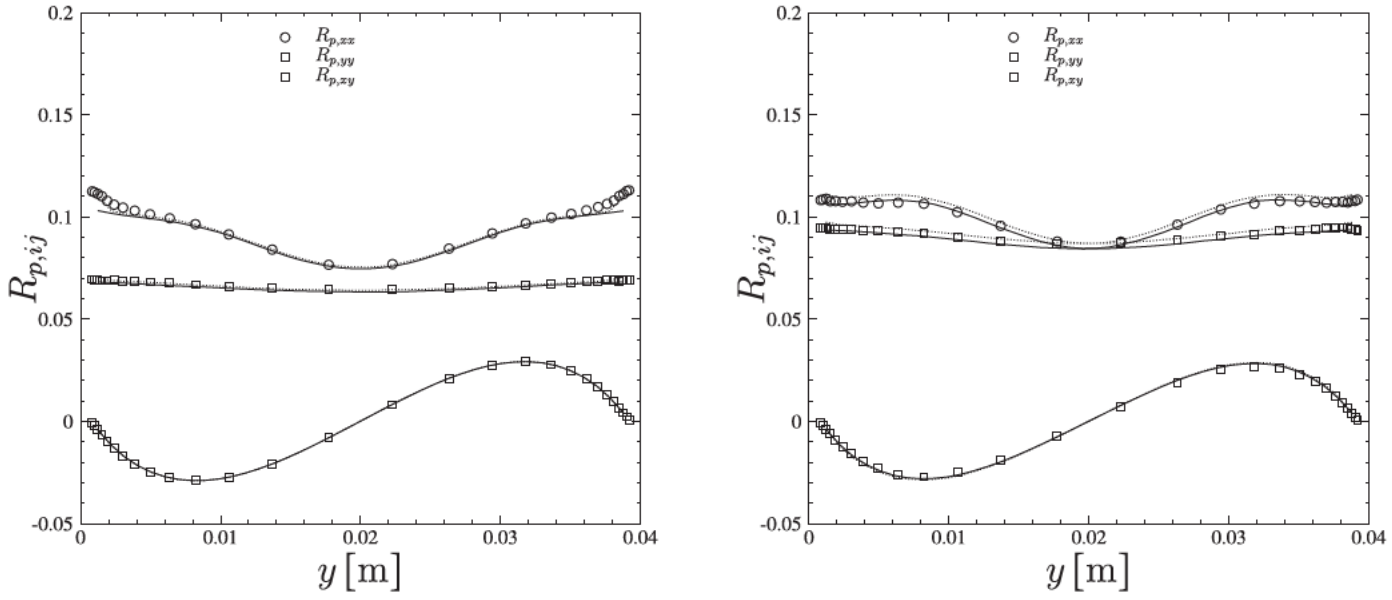

Fig. 18. Particle kinetic stress tensor for the case $d_p =$ 1500 μm. Left: $\overline{\alpha_p} = 1.4 \times 10^{-2}$ and right: $\overline{\alpha_p} = 4.1 \times 10^{-2}$. The symbols are the DPS results from Sakiz and Simonin (1998), the solid lines (_____) the standard DSMC results and the dotted lines (.....) the DSMC results with the "wall force" given by Eq. (34).

with,

$$C = 1 + \frac{\sqrt{32\pi}}{\tau_p^K}\left[\frac{2}{\tau_{fp}^F} + \frac{\sigma_c}{\tau_p^c}\right]^{-1} \tag{25}$$

We can notice that C is about 3 in the very dilute case ($\alpha_p = 1.2 \times 10^{-3}$) and is about unity in the less dilute case ($\alpha_p = 10^{-2}$). Figs. 9 and 10 show that the model proposed by Sakiz and Simonin (2001) improves significantly the moment method closure assumption.

5.2. Gas-particle momentum transfer terms

In the present paper, the focus is made on the case where the gas-particle interactions are driven only by the drag force. Except for the Stokes's regime, for very small particulate Reynolds numbers, the drag force dependence on the gas-particle relative velocity is nonlinear. In 1991, Simonin (1991) proposes to approximate the drag force by introducing the mean particle response time τ_{fp}^F, defined as $\frac{1}{\tau_{fp}^F} = 18\frac{\rho_f \nu_f}{\rho_p d_p^2}\left[1 + 0.15\langle Re_p\rangle^{0.687}\right]$ with $\langle Re_p\rangle = d_p \overline{\langle |\mathbf{v}_r|^2\rangle}/\nu_f$. The mean relative velocity being given by $\overline{\langle |\mathbf{v}_r|^2\rangle} = \overline{V_{r,m}V_{r,m} + \langle v'_{r,m}v'_{r,m}\rangle}$. Using this approximation, the drag terms in momentum and particle kinetic stress transport equations read

$$\left\langle \frac{F_{d,i}}{m_p} \right\rangle = -\frac{V_{r,i}}{\tau_{fp}^F} \tag{26}$$

$$\left\langle \frac{F_{d,i}}{m_p} u'_{p,j} \right\rangle + \left\langle \frac{F_{d,j}}{m_p} u'_{p,i} \right\rangle = -\frac{2R_{p,ij}}{\tau_{fp}^F} \,. \tag{27}$$

Later, Sakiz and Simonin (1998) proposed a model extension based on a Taylor expansion of the drag force near the averaged value $\langle |\mathbf{v}_r|^2\rangle$, leading to the drag term models:

$$\left\langle \frac{F_{d,i}}{m_p} \right\rangle = -\frac{V_{r,i}}{\tau_{fp}^F} + 2V_{r,m}\langle v'_{r,m}v'_{r,i}\rangle \left.\frac{\partial \Phi}{\partial X}\right|_{X=\langle |\mathbf{v}_r|^2\rangle} \tag{28}$$

$$\left\langle \frac{F_{d,i}}{m_p} u'_{p,j} \right\rangle + \left\langle \frac{F_{d,j}}{m_p} u'_{p,i} \right\rangle = -\frac{2R_{p,ij}}{\tau_{fp}^F} + 2V_{r,m}\left[V_{r,i}\langle v'_{r,m}v'_{r,j}\rangle + V_{r,j}\langle v'_{r,m}v'_{r,i}\rangle\right]\left.\frac{\partial \Phi}{\partial X}\right|_{X=\langle |\mathbf{v}_r|^2\rangle} \tag{29}$$

where the function $\Phi(X)$ is given by the drag law $\Phi(X) = -18\frac{\rho_f \nu_f}{\rho_p d_p^2}\left[1 + \left(\frac{d_p}{\nu_f}\right)^B AX^{B/2}\right.$. Here for the Schiller and Nauman's (see Eq. (3)) correlation the model coefficients are $A = 0.15$ and $B = 0.687$.

Figs. 11 and 12 show the drag terms in momentum and particle kinetic transport equations measured in case where $d_p =$ 406 μm and solid volume fraction is $\overline{\alpha_p} = 1.2 \times 10^{-3}$ and $\overline{\alpha_p} = 10^{-2}$. In momentum equation one can observe that, in axial direction, all model assumptions give nearly the same predictions. In the wall-normal direction, Eq. (17), the standard approach leads to a zero drag term in contradiction with DPS and DSMC results. In contrast, the model extension proposed by Sakiz and Simonin (1998) and computed with DPS data are in very good agreement with the numerical simulations.

For the particle kinetic stress transport equations, Figs. 11 and 12 show that the standard model overpredicts the drag term in the streamwise direction. Once again, the model extension taking into account large gas-particle drift clearly exhibits a better predictions. The extended model is also in better agreement with DPS and DSMC results for the shear component drag term. For the wall-normal and spanwise directions no significant improvements are found.

5.3. Inter-particle collision closure model

The analysis of inter-particle collision term effect starts with the inter-particle collision time scale τ_c which characterizes the collision effect on any moment. Fig. 13 shows the collision timescale measured from DSMC. For the small values of the mean particle volume fraction, one can observe that the collision timescale is maximum (small collision frequency) at the centre of the channel and decreases towards the walls (large collision frequency). For larger value of the mean particle volume fraction, the timescale is found more uniform across the channel.

For a given particle diameter, the collision timescale depends on two parameters: the local particle concentration and the local particle agitation. As shown by Fig. 5 the particle density number distribution across the channel exhibits a peak in the near-wall region and Fig. 6 shows large values of the agitation. Both effects leads to increase the collision frequency. In contrast at the centre of the channel, the solid volume fraction exhibits a peak but the particle kinetic energy agitation is small. The large value of the collision timescale in such a region means that the collision frequency is mainly controlled by the particle agitation.

In the framework of the kinetic theory, it is possible to derive an analytical expression for the inter-particle collision timescale,

$$\frac{1}{\tau_c} = n_p \pi d_p^2 \sqrt{\frac{16}{\pi}\frac{2}{3}q_p^2}\ . \tag{30}$$

For deriving Eq. (30), it has been assumed that the flow is sufficiently diluted ($\alpha_p < 5\%$) and the particles are very inertial with respect to fluid turbulence (Simonin et al., 2002) in order to consider that the radial distribution function is equal to unity. Fig. 13 compares the collision timescale measured from DSMC and the prediction given by Eq. (30). For the particles with the largest inertia, the moment closure modelling is in accordance with the DSMC results. In contrast, for the small particle diameters, it is observed that the model overestimates the collision frequency leading to a collision timescale smaller than the one measured from DSMC.

Eq. (30)is obtained by assuming that the single particle PDF is a Maxwellian distribution meaning that the fluctuating motion of the particles is assumed isotropic. Pialat (2007) proposed to take into account the anisotropy of the particle fluctuating motion by using an anisotropic Gaussian, or Richman, distribution. Such an approach leads to following expression of the inter-particle collision timescale,

$$\tilde{\tau}_c = \frac{\tau_c}{\frac{1}{2\sqrt{\frac{S+2}{3}}}\left[\sqrt{S} + \frac{\sinh^{-1}\left(\sqrt{S-1}\right)}{\sqrt{S-1}}\right]}. \tag{31}$$

where S is the coefficient representing the anisotropy of the fluctuating particle motion. Such a coefficient is given in terms of eigenvalues of the particle kinetic stress tensor $R_{p,\,ij}$. Basically, $S = \lambda_p/\lambda_q$ with λ_k the eigenvalues of $R_{p,\,ij}$ and $\lambda_p > \lambda_q$ (note that the derivation λ_q is assumed to be a double eigenvalue). As shown by Fig. 13 the Eq. (31) is in better accordance with DSMC results.

Following Grad (1949) and Jenkins and Richman (1985), in dilute particulate flows and using the molecular chaos assumption, the collision terms in particle kinetic stress tensor writes

$$\frac{1}{n_p}\mathcal{C}(u'_{p,i}u'_{p,i}) = -\frac{1-e_c^2}{3\tau_c}\ \frac{2}{3}q_p^2\delta_{ij} - \frac{\sigma_c}{\tau_c}\left(R_{p,ij} - \frac{2}{3}q_p^2\delta_{ij}\right) \tag{32}$$

with $\sigma_c = (1+e_c)(3-e_c)/5$. Fig. 14 compares the particle kinetic stress collision terms measured from DPS and DSMC with the moment closure model assumptions given by Eqs. (32) and (30) predictions. It can be observed that in the streamwise direction, R_{xx}, the collision term is negative in contrast with the collision terms in the wall-normal and spanwise directions. Such a behaviour is well known and represents the driving mechanism towards a Maxwellian distribution by inter-particle collision. Here the particle velocity variance in the x-direction is redistributed towards the two others directions without energy dissipation. Fig. 14 exhibits a very good agreement between the DPS and DSMC results and the models given by Eq. (32).

From DPS of vertical particle-laden channel flows, Sakiz and Simonin (1998) measured an accumulation of particles at a wall distance of the order of a particle diameter. They showed, from the wall-normal mean velocity equation balance Eq. (17), that this accumulation was due to the emergence of a collision term pushing the particles towards the wall and resulting from a shelter effect by the wall. To account for such a mechanism, they performed the theoretical computation of the collision term by considering a reduced space of integration accounting for the wall closeness and they obtained the following equation,

$$\begin{aligned}\frac{1}{n_p}\mathcal{C}(u_{p,y}) = &-\frac{1+e_c}{2}n_p d_p^2\left(\frac{2\pi}{3}q_p^2\right)\sin^2(\theta_m)\\ &-\frac{1+e_c}{6}n_p d_p^3\left(\frac{2\pi}{3}q_p^2\right)\left(1-\cos^3(\theta_m)\right)\\ &\times\left[\frac{2}{n_p}\frac{\partial n_p}{\partial y} + \frac{1}{q_p^2}\frac{\partial q_p^2}{\partial y}\right.\\ &\left.-\frac{1+e_c}{8}n_p d_p^2\sqrt{\pi}\left[R_{p,yy} - \frac{2}{3}q_p^2\right]\sin^2(\theta_m)\right.\\ &\left.\left(1+3\cos^2(\theta_m)\right)\right].\end{aligned} \tag{33}$$

In Eq. (33), θ_m is the parameter defining the sheltered space. If the wall is located at $y = 0$, $\cos(\theta_m) = \max(-1, 1/2 - y_p/d_p)$ with y_p the distance between the particle and the wall.

Fig. 15 shows that Eq. (33) predicts the non-zero value of the inter-particle momentum transfer in the near-wall region ($y_p < d_p/2$). It can also be observed that the Monte-Carlo method predicts a zero value because it assumes that the collision probability is not affected by the wall closeness. For taking into account the wall shelter, effect we basically proposed to add a force in the particle equation leading to Eq. (33) in the moment approach. However, an estimation from DPS results of the three term on the right hand side of Eq. (33) shows that the first one dominates the others. Hence, introducing, n_{wall} the wall-normal vector (oriented toward the core flow) and y_{wall} the position of the walls, the additional "wall force" that appears near the wall is taken into account in the Lagrangian framework as:

$$\frac{\mathbf{F}_{wall}}{m_p} = -|y - y_{wall}|\frac{1+e_c}{2}n_p d_p^2\left(\frac{2\pi}{3}q_p^2\right)\sin^2(\theta_m)\mathbf{n}_{wall}\ . \tag{34}$$

Figs. 16–18 show DSMC results with such a "wall force" for the case of $d_p =$ 1500 µm where the it is expected to be significant. It can be observed that the DSMC results are now in very good agreement with the DPS results even in the very near-wall region.

The effect of the "wall force" on the vertical particle velocity and on the mean particle kinetic stress tensor components are shown by Figs. 17 and (18). Fortunately, the "wall force" has a weak effect on those quantities and does not modify the good agreements that were obtained with standard DSMC method.

6. Conclusions

Direct Simulation Monte-Carlo (DSMC) of particles transported by a fully developed vertical turbulent channel flows are presented. Several diameters and mean particle volume fractions are considered. The main results of the paper can be split in two parts.

First, the comparison of the DSMC results with Discrete Particle Simulation (DPS) results shows the ability of the Monte-Carlo method to predict the particle-laden flow. The comparison between DSMC and DPS results is made for the particle number density, the mean vertical velocity and the second- and third-order velocity correlations. A very good agreement is found except for the particle number density in the very near-wall region. In such a region, the presence of the wall produces a wall shelter effect that drives the particles towards the walls. However, the application of an additional mean force, derived in the frame of the moment approach, allowed to reproduce accurately the increase of the particle concentration in the very near-wall region.

Second, the DSMC results have been used for testing the second order moment assumption for the third order velocity correlation, for the drag term, and for the collision terms. It was shown that, in the case of large fluid-particle mean slip velocity, the drag

term model proposed by Sakiz and Simonin (1998) is in very good agreement with the DPS or DSMC results.

Finally, even is some additional validation studies are required, the DSMC method can be straightforward extended for non-elastic frictional particle-particle and particle-wall collisions.

Acknowledgements

The authors would like to thank Dr. Philippe Villedieu from ONERA for fruitful discussions and help in the development of Monte-Carlo algorithm.

The authors would also like to thank Dr. Marc Sakiz for theoretical derivations and DPS statistics.

References

Arcen, B., Tanière, A., Oesterlé, B., 2006. On the influence of near-wall forces in particle-laden channel flows. Int. J. Multiphase Flow 32 (12), 1326–1339.

Babovsky, H., 1986. On a simulation scheme for the Boltzmann equation. Math. Methods Appl. Sci. 8, 223–233.

Balachandar, S., Eaton, J.K., 2010. Turbulent dispersed multiphase flow. Annu. Rev. Fluid Mech. 42 (1), 111–133. doi:10.1146/annurev.fluid.010908.165243.

Berlemont, A., Achim, P., Chang, Z., 2001. Lagrangian approaches for particle collisions: the colliding particle velocity correlation in the multiple particles tracking method and in the stochastic approach. Phys. Fluids 13, 2946–2956.

Berlemont, A., Simonin, O., Sommerfeld, M., 1995. Validation of inter-particle collision models based on large eddy simulation. In: Gas-Solid Flows, 228. ASME FED, pp. 359–369.

Bird, G.A., 1969. Direct numerical and the Boltzmann equation. Phys. Fluids 11, 2676–2681.

Capecelatro, J., Desjardins, O., 2013. An Euler–Lagrange strategy for simulating particle-laden flows. J. Comput. Phys. 238, 1–31. doi:10.1016/j.jcp.2012.12.015.

Chapman, S., Cowling, T., 1970. The Mathematical Theory of Non-Uniform Gases. Cambridge University Press.

Fede, P., Simonin, O., Villedieu, P., 2015. Monte-Carlo simulation of colliding particles or coalescing droplets transported by a turbulent flow in the framework of a joint fluid–particle pdf approach. Int. J. Multiphase Flow 74 (0), 165–183. doi:10.1016/j.ijmultiphaseflow.2015.04.006.

Fox, R.O., 2012. Large-eddy-simulation tools for multiphase flows. Annu. Rev. Fluid Mech. 44 (1), 47–76. doi:10.1146/annurev-fluid-120710-101118.

Grad, H., 1949. On the kinetic theory of rarefied gases. Commun. Pure Appl. Math. 2, 331–407.

Hanjalic, K., Launder, B., 1972. A Reynolds stress model of turbulence and its application to thin shear flows. J. Fluid Mech. 52, 609–638.

He, Y., Zhao, H., Wang, H., Zheng, C., 2015. Differentially weighted direct simulation Monte Carlo method for particle collision in gas–solid flows. Particuology 21, 135–145. doi:10.1016/j.partic.2014.05.013.

Ivanov, M., Rogasinsky, S., 1988. Analysis of numerical technics of the direct simulation Monte Carlo method in the rarefied gas dynamics. Sov. J. Num. Anal. Math. Modell. 3, 453–465.

Jenkins, J.T., Richman, M.W., 1985. Grad's 13-moments system for dense gas of inelastic spheres. Arch. Ration. Mech. Anal. 87, 355–377.

Nanbu, K., 1983. Stochastic solution method of the master equation and the boltzmann equation. J. Phys. Soc. Jpn. 52, 2654–2658.

O'Rourke, P.J., 1981. Collective Drop Effects in Vaporizing Sprays Ph.D. thesis. 1532-T

Pawar, S., Padding, J., Deen, N., Jongsma, A., Innings, F., Kuipers, J., 2014. Lagrangian modelling of dilute granular flow - modified stochastic {DSMC} versus deterministic {DPM}. Chem. Eng. Sci. 105 (0), 132–142. doi:10.1016/j.ces.2013.11.004.

Pialat, X., 2007. Développement Dune Méthode hybride Eulérienne-Lagrangienne Pour la Modélisation Numérique de la Phase Particulaire Dans les Écoulements Turbulents Gaz-particules. Ecole Nationale Supérieure de l'Aéronautique et de l'Espace Ph.D. thesis https://tel.archives-ouvertes.fr/tel-00224819v1.

Reeks, M.W., 1991. On a kinetic equation for the transport of particles in turbulent flows. Phys. Fluids 3 (3), 446–456.

Reeks, M.W., Simonin, O., Fede, P., 2016. Multiphase Flow Handbook. In: Computational Methods: PDF Models for Particle Transport Mixing and Collision in Turbulent Flows. CRC Press, pp. 79–284. doi:10.1201/9781315371924-3.

Riber, E., Moureau, V., Garcia, M., Poinsot, T., Simonin, O., 2009. Evaluation of numerical strategies for large eddy simulation of particulate two-phase recirculating flows. J. Comput. Phys. 228 (2), 539–564. doi:10.1016/j.jcp.2008.10.001.

Sakiz, M., Simonin, O., 1998. Continuum modelling and Lagrangian simulation of the turbulent transport of particle kinetic stresses in a vertical gas-solid channel flow. In: Proc. 3rd International Conference on Multiphase Flows.

Sakiz, M., Simonin, O., 1999. Development and validation of continuum particle wall boundary conditions using Lagrangian simulation of a vertical gas-solid channel flow. In: Proc. 8th Int. Symp. on Gas-Particle Flows, ASME Fluids Engineering Division Summer Meeting, FEDSM99-7898.

Sakiz, M., Simonin, O., 1999. Numerical experiments and modelling of non-equilibrium effects in dilute granular flows. In: Gatignol, R., Lengrand, J.C. (Eds.), Rarefied Gas Dynamics, Proc. of the 21st Int. Symp. on Rarefied Gas Dynamics, 1. Cépaduès Editions, pp. 287–294.

Sakiz, M., Simonin, O., 2001. Continuum modelling and Lagrangian simulation of massive frictional colliding particles in vertical gas-solid channel flow. In: Proc. 4th International Conference on Multiphase Flows.

Schiller, L., Naumann, A., 1935. A drag coefficient correlation. V.D.I. Zeitung 77, 318–320.

Simonin, O., 1991. Prediction of the dispersed phase turbulence in particle-laden jets. In: Proc. 1st Int. Symp. Gas-Solid Flows. ASME, pp. 197–206.

Simonin, O., 1996. Combustion and Turbulence in Two-phase Flows. Lecture Series 1996-02. Von Karman Institute for Fluid Dynamics.

Simonin, O., 2000. Statistical and Continuum Modelling of Turbulent Reactive Particulate Flows. Part 1: Theoretical Derivation of Dispersed Eulerian Modelling from Probability Density Function Kinetic Equation. Lecture Series 2000-06. Von Karman Institute for Fluid Dynamics, Rhodes Saint Genèse (Belgium).

Simonin, O., Février, P., Laviéville, J., 2002. On the spatial distribution of heavy particle velocities in turbulent flow: from continuous field to particulate chaos. J. Turbul. 3 (040), 1–18.

Sommerfeld, M., 2001. Validation of a stochastic lagrangian modelling approach for inter-particle collisions in homogeneous isotropic turbulence. Int. J. Multiphase Flow 27, 1829–1858.

Tanaka, T., Tsuji, Y., 1991. Numerical simulation of gas–solid two–phase flow in a vertical pipe on the effects of interparticle collision. In: P4th Symp. on Gas-Solid Flows, 121. ASME-FED, pp. 123–128.

Tsirkunov, Y.M., Romanyuk, D.A., 2016. Computational Fluid Dynamics / Monte Carlo Simulation of Dusty Gas Flow in a Rotor-stator Set of Airfoil Cascades. In: Array (Ed.), Progress in Propulsion Physics, 8, pp. 427–444. doi:10.1051/eucass/201608427.

Wang, S., Li, X., Lu, H., Yu, L., Ding, J., Yang, Z., 2009. DSMC prediction of granular temperatures of clusters and dispersed particles in a riser. Powder Technol. 192 (2), 225–233. doi:10.1016/j.powtec.2009.01.008.

Zaichik, L., Oesterlé, B., Alipchenkov, V., 2004. On the probability density function model for the transport of particles in anisotropic turbulent flow. Phys. Fluids 16, 1956–1964.